

## Development of a passive biped robot digital twin using analysis, experiments, and a multibody simulation environment

Christos Vasileiou, Aikaterini Smyrli, Anargyros Drogosis,  
Evangelos Papadopoulos\*

School of Mechanical Engineering, National Technical University of Athens, Athens, Greece

### ARTICLE INFO

#### Article history:

Received 8 January 2021

Revised 27 March 2021

Accepted 27 March 2021

Available online 28 April 2021

#### Keywords:

Passive bipedal walking  
Design methodology  
Digital twin  
Multibody dynamics  
Simulation design  
Experimental validation

### ABSTRACT

This paper presents a unified framework for the design and development of a passive biped robot and of its digital twin. A serial procedure is followed starting from the system's physical description, continuing to the dynamic analysis of independent models, and concluding with an experimental validation. The biped's mechanical model is tailored to preserve passive walker key functionalities without sacrificing design simplicity. The mechanical model gives rise to a mathematical model that describes the biped's gait, and to a multibody dynamics model of the biped. A passive biped robot prototype is developed based on the model. The prototype is equipped with a wireless sensor measuring system to enable data acquisition. The highlight of this work is the high degree of coincidence achieved between the passive response of the numerically simulated mathematical model, the response obtained by a multibody dynamics simulation, and the experimentally obtained response of the physical passive walking robot. This finding verifies the simulation methods used and encourages the use of a carefully designed digital twin in the design iterations involved in the development of walking robots.

© 2021 Elsevier Ltd. All rights reserved.

### 1. Introduction

The need for a consistent study of the human gait has led the research community to the development of mechanical models of walking and biped robots. Passive dynamic walkers were first introduced by McGeer in his theoretical and experimental work [1]. From there on, many researchers investigated different configurations for biped robots, in both theoretical and experimental approaches. Theoretical studies have focused on the effect of design parameters on the passive gait of biped robots. McGeer studied the effects of mass distribution, circular foot radius, and damping elements [1], while Alexander investigated the leg axial compliance [2]. Many researchers have combined such elements in models of varying complexity, and via simulations, they have exerted useful results with direct conclusions about robot or even human bipedal gait [3–7]. This type of effort can be undermined by common occurrences when using a numerical simulation, such as improper modelling decisions, simulation coding errors, or even typical numerical errors.

A more robust route to obtaining gait insight is building a robot and performing experiments. Although usually the biped robot's design is loosely based on previous analytical studies of simple models or templates, its dynamics are generally more

\* Corresponding author.

E-mail address: [egpapado@central.ntua.gr](mailto:egpapado@central.ntua.gr) (E. Papadopoulos).

## Nomenclature

SSP	Single Stance Phase
DSP	Double Stance Phase
HS	Heel-Straike
TO	Toe-Off
$\theta$	Stance leg angle
$L_1$	Stance leg length
$\psi$	Swing leg angle
$L_2$	Swing leg length
$h$	Distance between foot centres
$F_N$	Normal ground force in Adams
$F_k$	Stiffness component of $F_N$ in Adams
$F_c$	Viscous component of $F_N$ in Adams
$d$	Max. ground penetration in Adams
$V_s$	Stiction transition velocity in Adams
$V_d$	Friction transition velocity in Adams
$\mathbf{q}$	Generalized coordinate vector
$\mathbf{x}$	State variable vector
$\mathbf{M}$	System mass matrix
$\mathbf{C}$	System Centrifugal & Coriolis vector
$\mathbf{K}$	System elasticity vector
$\mathbf{s}$	Constraint vector
$\lambda$	Constraint force vector
$p$	Phase switching variable
$x_0$	Stance foot initial position
$z$	Foot position variable in Adams
$k_c$	Stiffness of $F_N$ in Adams
$c$	Variable damping of $F_N$ in Adams
$e$	Force exponent of $F_N$ in Adams
$\mu_s$	Static friction coefficient in Adams
$\mu_d$	Dynamic friction coefficient in Adams

complex. McGeer accompanied his theoretical results with a simple passive biped prototype on which he performed gait experiments [1]. Collins and Ruina designed and built a biped robot, which consists of a torso, hip knee and ankle joints, and special feet for lateral stabilization, which allowed them to study its energetic efficiency [8]. Wisse et al. increased the structural complexity by using McKibben muscles to power the hip and knee joints of the Mike robot [9]. Corral et al. studied the forward and inverse dynamics of a quasi-passive biped robot in their theoretical work [10] and validated their results by building and testing an experimental prototype [11]. Biped robots with actuators acting as active elastic [12] or damping [13] elements have also been built based on the analysis of mathematical models. Finally, state-of-the-art robots, highly complex in their design, have been developed and studied, such as the 13 DoF, passivity-inspired ATRIAS [14], or the 43 DoF humanoid robot WABIAN-RIV [15].

Bipedal walkers belong to a distinctive case of dynamic systems: due to their highly nonlinear, hybrid dynamics, their gait is often subject to bifurcations and they have been shown to present chaotic behaviour [16,17]. Moreover, their dynamics heavily depend on the impact and friction properties of their feet contact with their ground, the modelling and simulation of which often prove challenging [18]. These dynamic characteristics lead to potentially large orbital divergence following a small perturbation or design alteration which can result in inconsistencies in simulation and experimentation results, especially in passive systems without corrective actuation schemes. Therefore, in such systems, it is especially important that steps be taken to limit the sources of such perturbations or design alterations, in order to increase confidence in the results obtained by any method.

Experimental prototypes generally vary in their degree of resemblance to the simple mechanical models used for the theoretical studies: it is thereby expected that the experimental results may converge or diverge from the simulation predictions according to the degree of similarity between the robot and its model. **Therefore, one method to limit the dynamical divergence between simulation and reality is to increase the degree of resemblance between the robot and the model.**

The use of simpler robot designs facilitates the description of the gait dynamics by a simple model and leads to comparable results between simulations based on analytical mathematical models, and experiments [19–21]. Studies of simple models allow researchers to evaluate their modelling decisions, such as the implementation of system constraints, or the validity of assumptions, and to optimize the simulation process for more complex models.

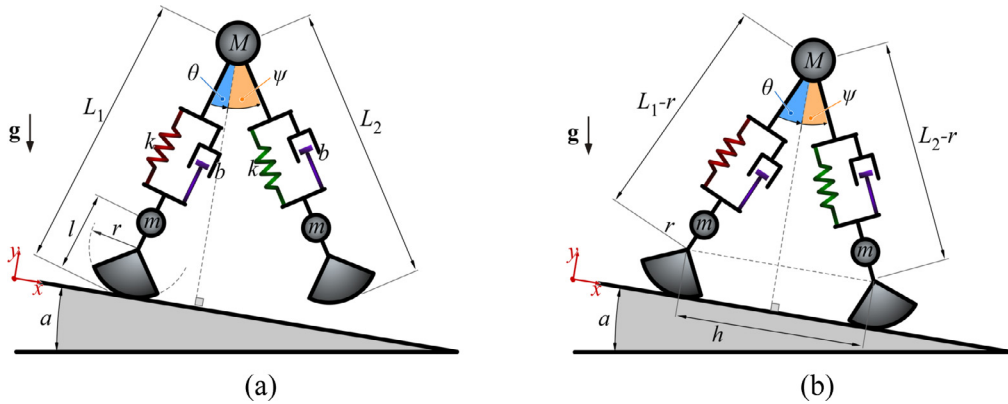


Fig. 1. Schematic of the biped's mechanical model during (a) the SSP (b) the DSP.

Another method towards fine-tuning the simulation process to closely match the physical reality is a multibody simulation of the robot's dynamics: an intermediate step between the mathematical model and the prototype. In this method, a 3D body model of the robot is simulated for its passive walk in a dedicated multibody simulation software. This method requires less effort than building a robot and performing experiments and offers results that are less partial to modelling or coding errors compared to a numerical simulation of analytical models but can be affected still by integration and round-off errors. There have been notable studies on the simulation of passive walkers in multibody programs [22,23]. However, to this date, a sufficiently high degree of closeness between mathematical models and multibody dynamics simulations of passive biped robots has not been achieved [23].

Some researchers have combined the above approaches and used results obtained via a mathematical model simulation, a multibody dynamics simulation, and experiments performed using a prototype to achieve a biped robot design [24–27]. These works have provided some useful insight on the steps followed during the design and experimental process, but their main objective has been the robot design optimization. This leaves a gap in the literature of passive biped robots, regarding the steps required to build a mathematical model and a multibody dynamics simulation that will match each other adequately, and with the experimental data obtained from a physical passive biped robot.

This work presents in detail the process of evolving a biped from a simple analytical model to a manufactured robot prototype. The developed method incorporates the comparison and unified study of the results from intermediate stages of the development and facilitates the evaluation of the effects of minor design alterations in each step of the process. In addition, the experimental setup and the data acquisition system used in the experiments is presented in detail. Conclusions are drawn regarding the adequacy of each of the methods used in evaluating the biped's gait. Expanding our previous research work, the main contribution of this paper is that it provides a complete methodology that successfully translates a simple mechanical model to its twin working prototype: through mathematical analysis, numerical simulations, multibody dynamics simulations, and experiments. By achieving the replication of the nonlinear hybrid passive dynamics of an unactuated double pendulum biped across independent approaches, this work provides useful insights about the suitability of individual simulation methods in approximating the behaviour of such systems.

## 2. Mathematical modelling and simulation

With the aim of investigating the best practices towards achieving a dynamic match between model and robot, the modelling process must take into account the dominant dynamic modes of the biped robot and include them in the model's dynamics, thus eliminating this source of dynamic divergence. As a result, the biped model studied in this paper incorporates some of the key structural elements that are present in passive biped robots.

### 2.1. Derivation of the model

The biped, see Fig. 1, is modelled as a double pendulum, with two legs of natural length  $L_{nat}$  joined together at the hip of the biped, where the lumped body mass  $M$  is located. Each leg foot is of circular shape with radius  $r$  and has mass  $m$  located at distance  $l$  from its bottom. The legs are given an axial degree of freedom, upon which elastic and damping elements of constants  $k$  and  $b$  respectively act. These are present even in rigid robots, as most materials present some degree of elasticity and damping. Table 1 presents the model's parameter values.

The biped's configuration is defined by its two legs' rotation angles,  $\theta$  and  $\psi$ , and their corresponding lengths,  $L_1$  and  $L_2$ . These constitute the generalized coordinate vector  $\mathbf{q}_{4 \times 1}$

$$\mathbf{q} = [\theta, L_1, \psi, L_2]^T \quad (1)$$

**Table 1**  
Biped model's design parameters.

Parameter	Symbol	Value
Hip Mass	M	0.316 kg
Leg length	L <sub>nat</sub>	0.333 m
Foot mass	m	0.335 kg
Foot radius	r	0.083 m
Foot CoM	l	0.100 m
Spring constant	k	2800.00 N/m
Damper constant	b	58.350 Ns/m

which, combined with its time derivative,  $\dot{\mathbf{q}}$ , defines the biped's state vector  $\mathbf{x}_{8 \times 1}$

$$\mathbf{x} = [\mathbf{q}^T, \dot{\mathbf{q}}^T]^T \quad (2)$$

During walking, the biped always has at least one of its legs in contact with the ground; we call this the *stance leg*; its state is defined by the state variables  $\theta$  and  $L_1$ . The second leg, called the *swing leg*, is described by  $\psi$  and  $L_2$ . The swing leg can either be swinging forward, in a phase called the *Single Stance Phase* (SSP), or it can be in contact with the ground, marking the *Double Stance Phase* (DSP). The first moment of the DSP is the *Heel Strike* (HS) event when the swing leg first meets the ground, and the last is the *Toe Off* (TO) event, when the leg previously acting as a *stance leg* is lifted from the ground.

During the DSP, the swing leg is constrained in its contact with the floor. There are two constraints acting on it. The first is the *foot-on-ground constraint*:

$$r + (L_1 - r) \cos \theta - (L_2 - r) \cos \psi = r \Rightarrow \\ s_1 \stackrel{\Delta}{=} (L_1 - r) \cos \theta - (L_2 - r) \cos \psi = 0 \quad (3)$$

The second constraint is the *rolling contact constraint*, which assumes that there is no slip between the foot and the floor:

$$h = h_{HS} - r(\theta - \theta_{HS}) - r(\psi - \psi_{HS}) \Rightarrow \\ s_2 \stackrel{\Delta}{=} h_{HS} - h - r(\theta_{HS} - \theta) - r(\psi_{HS} - \psi) = 0 \quad (4)$$

where  $h$  is the distance between the two circular foot centres, as shown in Fig. 1(b), and the subscript HS marks the values of the variables at the HS instance.

Let the vector of forces corresponding to the constraints  $\mathbf{s} = [s_1, s_2]^T$  be the  $2 \times 1$  vector  $\lambda = [\lambda_1, \lambda_2]^T$ . The force component  $\lambda_1$  originates from the first constraint  $s_1$  and is equal to the friction force component acting on the swing leg due to its contact with the ground. The second,  $\lambda_2$ , is the normal contact force component. The ground contact force  $\lambda$  acts on the biped's generalized variables through the Jacobian matrix  $\Pi_{4 \times 2}$ :

$$\Pi = \left( \frac{\partial \mathbf{s}}{\partial \mathbf{q}} \right)^T = \mathbf{0} \quad (5)$$

The equations describing the biped's dynamics can be written in the form:

$$1 \quad \mathbf{M}(\mathbf{q})\ddot{\mathbf{q}} + \mathbf{C}(\mathbf{q}, \dot{\mathbf{q}})\dot{\mathbf{q}} + \mathbf{K}(\mathbf{q}) + p\Pi\lambda = \mathbf{0} \\ 2 \quad p\mathbf{s} = \mathbf{0} \quad (6)$$

where  $\mathbf{M}_{4 \times 4}$  is the biped's mass matrix,  $\mathbf{C}_{4 \times 4}$  is a matrix containing centrifugal and Coriolis terms,  $\mathbf{K}_{4 \times 1}$  is the stiffness vector containing elastic spring forces and  $p$  is a switching variable. The solution algorithm switches between the walking phases every time a HS or TO event occurs, by setting the switching variable to  $p=0$  during the SSP where the swing leg is unconstrained, and to  $p=1$  for the DSP where there is contact of the swing leg with the ground.

Fig. 2 presents the normal and frictional force components of  $\lambda$  during a foot contact with the ground. The foot studied here is initially (at  $t=0$ ) in swing, therefore it is not subject to any ground reaction forces. The velocity of the biped's swing foot with respect to the ground causes an impact and at HS the switching variable gets switched to  $p=1$ . As can be observed in Fig. 2, at DSP, instantaneous impact forces result in order to satisfy the algebraic constraints imposed at that instant and to decelerate the biped's foot. After the complementary leg is lifted from the ground, the DSP is terminated, and the leg studied here acts as a stance leg. At the next DSP, when the complementary leg hits the ground, the normal force, component  $\lambda_1$ , gradually decreases to zero, at which point TO occurs and the switching variable is set to  $p=0$ .

Methodologically, the application of the ground contact constraints  $\mathbf{s}$  in (6) when  $p=1$  introduces the force components  $\lambda_1$  and  $\lambda_2$  within the force vector  $\lambda$ , and simultaneously constraints their value so that the algebraic constraints (3) and (4) are satisfied; note that the latter constrain the motion of the foot on the ground but do not specify a dynamic contact model for this interaction. Instead, the force vector  $\lambda$  is viewed here as a vector of Lagrange multipliers that correspond to the constraints in  $\mathbf{s}$ . The practice of using Lagrange multipliers to model contacts in dynamic systems minimizes the

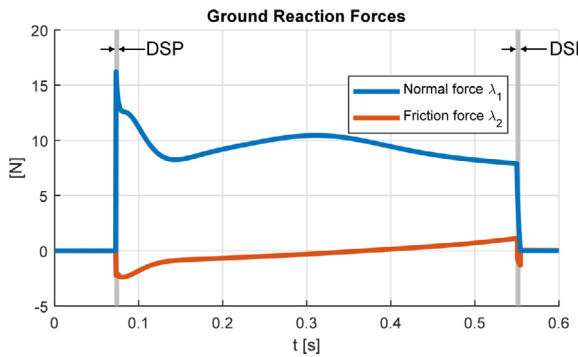


Fig. 2. Ground reaction forces for a foot in MATLAB.

computational effort by reducing the overall stiffness of the system. On the other hand, this loss of stiffness could potentially lead to false predictions made by simulations of the mathematical model, since the ground reaction forces are essentially a periodic force input that acts on the passive dynamics. For this reason, some studies have developed detailed and optimized analytical expressions for the ground contact forces in bipedal walking [28,29]. In this study, the results obtained with the developed system are then validated by independent simulations of a different model that incorporates a contact mechanics model; therefore, the efficiency and validity of this approach will be put to the test.

## 2.2. Simulation environment

The simulations of the mathematical model of the biped and the post-processing of the results were conducted in MATLAB. During the SSP when  $p=0$ , (6) reduces to a  $4 \times 4$  system of 2<sup>nd</sup> order Ordinary Differential Equations (ODEs). The ODEs describing the SSP can be integrated by most ODE solvers in MATLAB; in this study, the moderate-stiffness `ode23` was selected.

However, during the DSP, the system in (6) is a  $6 \times 4$  system of Differential Algebraic Equations (DAEs). The algebraic equations appended to the system do not contain acceleration terms, and therefore the state-space representation of the system has a singular state matrix, which cannot be inverted to solve for the states. In fact, the DAE system is of index 2, as the algebraic Eqs. (3) and (4) would need to be differentiated twice to produce acceleration terms that would populate the state matrix and allow for its inversion. A double differentiation of these constraints, which would technically reduce the system to a set of ODEs, was found to eliminate the first order terms of  $s$  in (6), resulting in a set of constraints that do not describe rolling without slipping. Due to this reason, the DAE system cannot be reduced to an ODE system. However, a single differentiation of the constraints is possible without loss of functionality. This is performed, reducing the DAE index to 1.

The index reduction is essential to simulating the DAE system, as MATLAB does not offer solvers for DAEs with an index greater than 1. Moreover, only a few of MATLAB's solvers are able to perform index 1 DAE integration. Out of these, the `ode15s` solver was found to be the most suitable for the stiff dynamics of the DSP, where the hip is supported by the two stiff legs in contact with the ground.

The system was studied to identify its stable repetitive solutions that constitute a stable passive walking cycle. More details about the model and methods used to locate walking cycles of the biped can be found in [30]. Table 1 presents the parameter values selected for the final design. These parameters were selected using MATLAB to optimize the design for passive gait stability. To do this, the gait of the biped was expressed in the form of a linearised Poincaré map, which was then used to evaluate the biped's stability via calculation of the linearised system's eigenvalues. A Newton-Raphson method was used to reach an optimal parameter set, for which the eigenvalues are minimum in magnitude, similarly to the process followed in [30]. The theoretically optimal parameters were later used to guide the design of the constructed robot and finally, their values were fine-tuned to measurements obtained from the robot.

## 2.3. Post-processing of results

The results of a numerical simulation in MATLAB can be post-processed to obtain records not only of the state variables, but also of different measures that might be of interest for comparison and validation purposes. For example, Fig. 8 presents hip displacement and velocity results obtained from post-processing simulation results. To obtain these measures, kinematic or dynamic relations are applied to the model.

To illustrate this, Eq. (7) is used to calculate the biped's hip displacements in the  $x$  and  $y$  direction of Fig. 1 (a):

$$\begin{aligned} x_{\text{hip}} &= x_0 + r\theta + (L_1 - r) \sin\theta \\ y_{\text{hip}} &= r + (L_1 - r) \cos\theta \end{aligned} \quad (7)$$

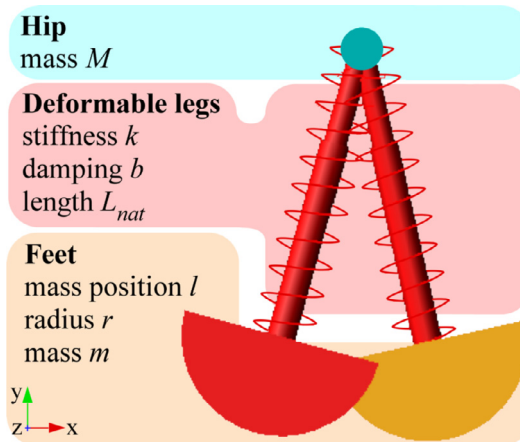


**Fig. 3.** The simplified biped model in MSC Adams. The biped moves in the  $x$ - $y$  plane and rotates about the  $z$  axis. Motion in the other directions is constrained to ensure identical conditions among the numerical simulations in MATLAB and MSC Adams.

In (7),  $x_0$  is the position of the biped's stance foot centre for  $\theta=0$  of the current step, and it is used for continuity purposes during plotting: its value is updated at the beginning of each step to match the position of the new stance leg. Similarly, for the hip velocities:

$$\begin{aligned}\dot{x}_{\text{hip}} &= r\dot{\theta} + \dot{L}_1 \sin \theta + \dot{\theta}(L_1 - r) \cos \theta \\ \dot{y}_{\text{hip}} &= \dot{L}_1 \cos \theta - \dot{\theta}(L_1 - r) \sin \theta\end{aligned}\quad (8)$$

The results of interest are always a function of the state vector,  $\mathbf{x}$ , which is calculated as a function of time when the dynamics are solved. In this manner, dynamic information about any point of interest on the biped is available, given the time solution of the state vector  $\mathbf{x}$ .

To minimize the extent of integration errors, and to increase confidence on the simulated results of the state vector's value over time, the tolerances in the solver options offered by MATLAB were carefully selected. Too large tolerances would allow large integration errors, while too small tolerances would lead to a large increase in solver steps, increasing the overall rounding error accumulated over the same time. After experimenting with this trade-off, we have set both the relative and absolute tolerances in MATLAB equal to  $10^{-7}$ .

#### 2.4. Conclusion about the method

Obtaining a mathematical model for the description of gait dynamics facilitates the design process, as it enables the evaluation of many design options at once, bypassing the need to construct a prototype at each iteration. The model can be simulated in a user-defined script, enabling the personalization of the process but introducing at the same time the risk of erroneous results due to programming or numerical errors. Therefore, the mathematical model is a very useful tool in the initial steps of the design process, but its results should be cross-validated using additional methods to ensure their validity, before constructing the real robot.

### 3. Dynamics simulations and comparisons

Simulations with a multibody software, such as MSC Adams, offer the advantage that they can incorporate several models of varying complexity: from simple stick-figure models to detailed 3D ones. In this section, a simplified model is built to match the mathematical model and to validate the results obtained by it.

#### 3.1. Simplified model in MSC Adams

The simplified model of the biped, shown in Fig. 1 and described in (6), is translated to the multibody system of Fig. 3, using the simulation environment MSC Adams. The model is built in three dimensions but is constrained to move in a two-dimensional plane. The walking motion is realized here with the use of a rotational joint at the hip and two prismatic joints along the direction of the legs, upon which act the spring and damper.

#### 3.2. Dynamic divergence and its causes

A high degree of dynamic resemblance between the two model descriptions is expected since both models simulate the same dynamic system. However, it has been suggested that the dynamic resemblance between mathematical and multibody

dynamics simulations is limited in passive dynamic walker studies [23]. It was found that this is mainly caused by differences in model description: specifically, the biped's impact and subsequent contact with the ground was implemented in the previous section by imposing Lagrangian constraints to the biped's dynamic equations; on the other hand, the multibody dynamics simulation program MSC Adams has a dedicated "contact" function that can be used to model the interaction with the ground. Another source of dynamic divergence are the different solvers available in each computational environment and their respective settings: these can introduce artefacts in the simulation results and mislead the design process. The dynamic divergence introduced by these factors, albeit small, can be amplified in systems capable of chaotic behaviours, as is the double pendulum, and lead to completely different simulation outcomes.

Next, the process of comparing the biped walker in MSC Adams to the MATLAB model will be demonstrated. Special care is taken to avoid solver-related artefacts by tuning carefully the simulation parameters. Most importantly, the main sources of dynamic divergence between mathematical and multibody dynamics modelling are investigated, yielding a set of guidelines for future comparison studies. Also, the results of this comparison will guide the design of the experimental prototype, as they determine the degree of complexity allowed in the detailed 3D design before dynamic convergence is lost.

### 3.3. Normal force model in MSC Adams

The main discrepancy between the mathematical and the multibody dynamics model of the biped robot is the interaction of the biped with the ground. As mentioned above, Lagrangian constraints are used to model the effect of ground interaction in MATLAB's numerical simulations. On the other hand, a detailed contact model is implemented in MSC Adams. This model consists of a normal and a friction force acting on the contact point between the foot and the ground. The normal force model used in Adams is discussed in this section, while the model used for the frictional component is addressed in the next one.

Several contact mechanics models have been developed for the estimation of the normal contact force between two solids that interact. MSC Adams includes -by default- two such models for a contact's normal force computation. The first option is called "Restitution" and allows the user to energetically characterize an impact by setting the value of the impact's coefficient of restitution. For a perfectly elastic collision this coefficient is equal to 1 and for a perfectly inelastic collision it is equal to 0. The second model, called "Impact," utilizes a nonlinear viscoelastic model for the contact between the two bodies. It is based on Hunt-Crossley's representation of the normal contact force and includes elastic and hysteretic dissipation elements [31,32]. The model is widely used and adapted for various cases of inelastic collisions in contact mechanics [33–36], and includes a set of four tuning parameters, which enable for a detailed description of the normal contact force.

More specifically, the model attributes viscoelastic properties at the normal force  $F_N$  applied on the foot from the ground and is described by a branch function:

$$F_N = \begin{cases} 0, & z > z_0 \\ \underbrace{k_c(z_0 - z)^e}_{F_k} - \underbrace{c(z)\dot{z}}_{F_c}, & z \leq z_0 \end{cases} \quad (9)$$

where  $z$  is a position variable,  $z_0$  specifies the trigger position at first contact,  $k_c$  is the contact stiffness,  $e$  is the force exponent, and  $c(z)$  is the variable damping of the impact.

Inspection of (9) shows that for  $z > z_0$ ,  $F_N$  is zero, corresponding to configurations where there is no contact of the foot with the ground, as is true during a leg's swing phase. For  $z \leq z_0$  where the contact is active,  $F_N$  is composed of two parts: the first term is the stiffness component  $F_k$ , while the second part introduces a viscous force component  $F_c$ , which is a function of the speed of penetration.

Fig. 4 aids in visualizing (9). Fig. 4a illustrates the effect of the force exponent  $e$  on the impact's stiffness: for  $e = 1$  the stiffness of the ground is constant and the ground acts as a linear spring. For contact mechanics,  $e$  is always greater than 1, introducing a hardening stiffness nonlinearity. Fig. 4b presents the dependence of the impact's damping on the position variable  $z$ . The damping achieves its maximum value  $c=c_{max}$  after a penetration depth  $d$ , as measured from the trigger position  $z_0$ . The gradual increase of  $c$  in the plot is used to avoid non-continuities in the normal force  $F_N$ .

The parameters of the contact force model enable the simulation of the biped's gait on various surfaces. The main parameters that configure the normal force are the ground stiffness  $k_c$ , the maximum damping coefficient  $c_{max}$ , the force exponent  $e$ , and the maximum penetration depth  $d$ . Aiming at evaluating the resemblance between the multibody dynamics model's contact formulation to the mathematical model's ground constraints, an investigation of the contact model's parameters was conducted. Fig. 5 compares the normal forces of the gait on the custom surface, as a function of various contact parameter sets. Each column presents the normal forces that result from changing one parameter from its default value, while keeping the others at their default values. The force responses corresponding to the default parameter set are enclosed in a grey box.

As can be seen in Fig. 5, a small change in the value of  $k_c$  results in an improvement of the contact force model's resemblance to the ground force that was calculated by the mathematical model and presented in Fig. 2, while still maintaining realistic contact parameter values. Therefore, this parameter set is used for the comparison of the multibody dynamics model in MSC Adams to the mathematical model in MATLAB. The same parameter set will be used also for later comparisons of a detailed CAD model in Adams with the experimental prototype.

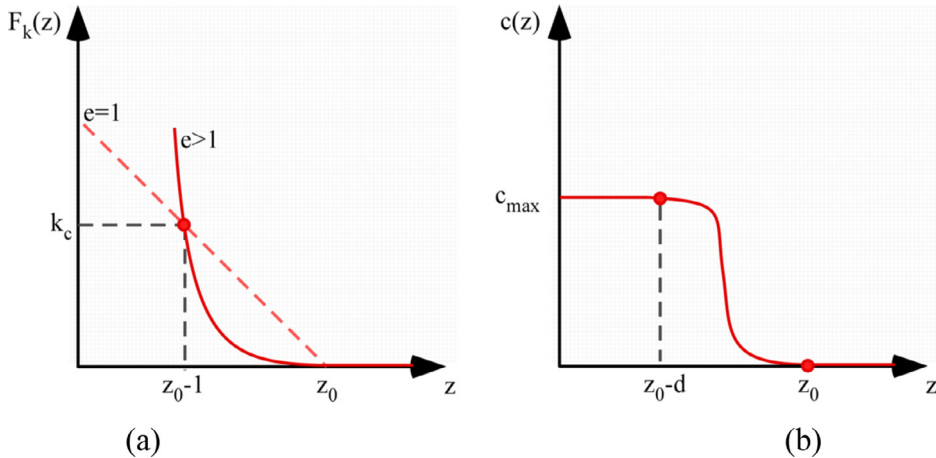


**Fig. 4.** Visualization of the ground contact force parameters. (a) Dependence of stiffness force  $F_k$  on the force exponent  $e$ . For contact mechanics,  $e > 1$ . (b) Gradual increase of contact damping with penetration depth, until  $c_{max}$ , reached at penetration  $d$ .

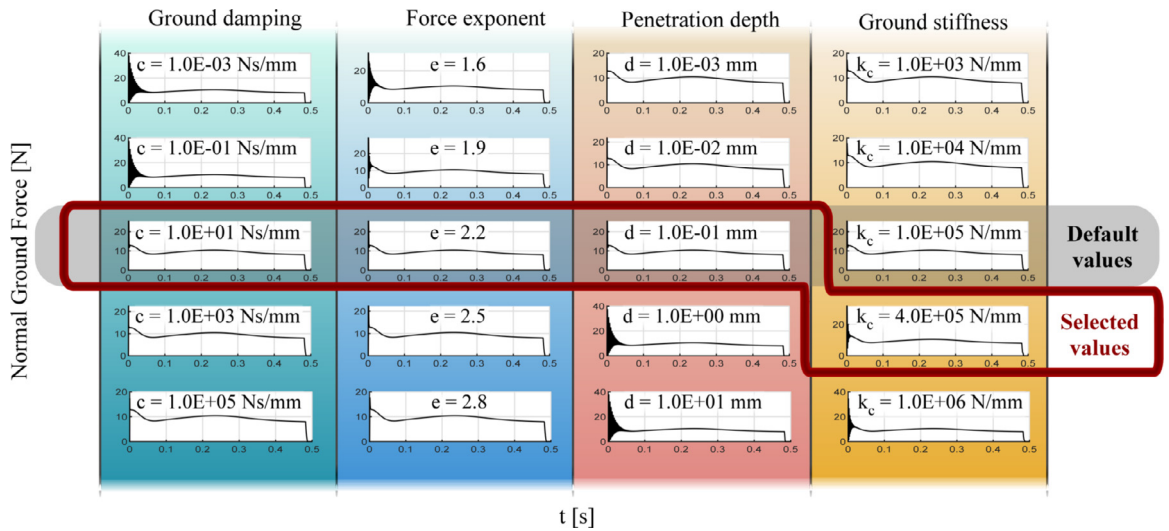


**Fig. 5.** Impact of contact parameter deviations on foot normal force in MSC Adams. Starting with the default values in the grey box, one parameter is altered per column to investigate the behavior of the foot normal force. Large changes in the default parameter values lead to oscillating behaviors that are not present in the mathematical model. A realistic behavior is observed in the set enclosed with an outline, which is selected as the contact parameter set for the comparisons that follow. (For interpretation of the references to colour in this figure legend, the reader is referred to the web version of this article.)

### 3.4. Friction model in MSC adams

An equally important factor affecting the closeness between the mathematical and multibody dynamic models is the definition of the friction force acting between the feet and the ground. The friction force is a substantial component of the contact model, as it affects the ability of the foot to perform pure rolling without slipping during its contact with the ground. MSC Adams includes a modified continuous Coulomb friction model that is able to approximate stick-slip friction phenomena in the simulations performed.

The frictional force of the foot's contact with the ground,  $F_T$ , is of the general form

$$F_T = \mu(v) \cdot F_N \quad (10)$$

where  $\mu$  is the coefficient of friction and  $F_N$  has been calculated in (9). The coefficient of friction  $\mu$  generally depends on the relative velocity between a foot and the ground,  $v$ .

More specifically, the frictional model used in Adams includes an approximation of the Stribeck effect, but it offers a numerical advantage to the classic Stribeck curve by avoiding the discontinuity at zero relative velocity [37–39]. It has four tunable coefficients. These include the static and dynamic friction coefficients, defined by  $\mu_s$  and  $\mu_d$  respectively, as well as the *stiction* transition velocity  $v_s$  and the *friction* transition velocity  $v_d$ . The frictional state of the contact depends on the

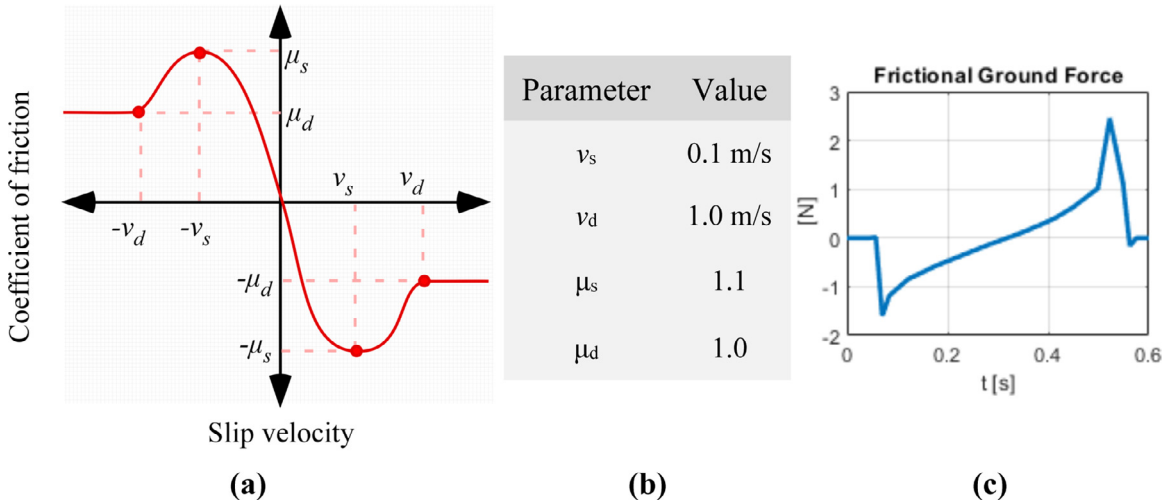


**Fig. 6.** (a) Coulomb friction model used in MSC Adams. The model enables the study of stick-slip friction scenarios. (b) Parameter values used. (c) Frictional ground reaction force in MSC Adams for a step of the biped.

contact's relative velocity: for small relative velocities the friction is considered static, whereas for larger relative velocities the contact transitions to a slipping state where dynamic friction applies. Fig. 6 presents the friction model used in Adams (a,b).

The developed mathematical model in MATLAB assumes pure rolling of the foot on the ground. For this to hold during the simulations and experiments, the friction on the foot must remain static. This is achieved by selecting material combinations that present a high static friction coefficient  $\mu_s$ . In the MSC Adams simulations, a value of 1.1 was set for  $\mu_s$ , which is also achievable by the experimental prototype, as it is a typical value for rubber foot soles on various walking surfaces. Accordingly, the dynamic friction coefficient was set to be slightly smaller than the static one. The rest of the friction model parameters were set to match the MATLAB model: by using trial-and-error, the response of the passive walker in MSC Adams was simulated for several values of the parameters. It was observed that for small to moderate changes of the stiction and friction transition velocities with respect to the default, the behaviour of the walker was not affected. Therefore, it was decided to set the stiction and friction transition velocities to their default values set by MSC Adams. These values can be found in Fig. 6(a).

The resulting frictional force applied to a foot from the ground in MSC Adams is presented in Fig. 6(c), which validates the frictional force estimation performed by  $\lambda_2$  in the MATLAB model, see Fig. 2.

### 3.5. Walking simulations

Having analysed the structural similarities and differences between the two models, the next step is to select a suitable MSC Adams solver, yielding reliable simulation. As reasoned in Section 2, a stiff solver is appropriate for this system. For the numerical simulation in MATLAB, the `ode15s` solver was used; the corresponding solver in MSC Adams is the GSTIFF integrator, which is a variable order, variable step size integrator that provides fast and accurate results for a wide range of motion analysis applications, including stiff problems. The Adams solver was modified to have an integration tolerance of  $10^{-6}$ , to limit deviation due to error accumulation. In addition, the solver's time step is set to change depending on the phase of the biped. For example, smaller time steps are used around the impact events than those used for the rolling motion: this is achieved using a simulation script.

Fig. 7 provides a series of motion snapshots. The goal is to compare the gait of the two biped models presented so far. The simplified biped model achieves stable walking in a negative slope of 2°. As mentioned earlier, the two models have been developed independently in MATLAB and MSC Adams, and describe the same behaviour, but with a few differences. A comparison between them allows the evaluation of the effectiveness of the Lagrangian constraints in simulating contact dynamics in mathematical models. Indeed, this comparison is presented in Fig. 8, where key results of the simulations are superposed in hybrid plots. In particular, hip displacement and hip velocity in the x and y direction of motion are recorded for each model and found to be almost identical. Similarly, converging results have been obtained for various other determinants of gait, but are spared here. The big resemblance among the two models verifies the modelling decisions made in developing both models and presents encouraging results regarding the modelling of a dynamic system in two independent ways.

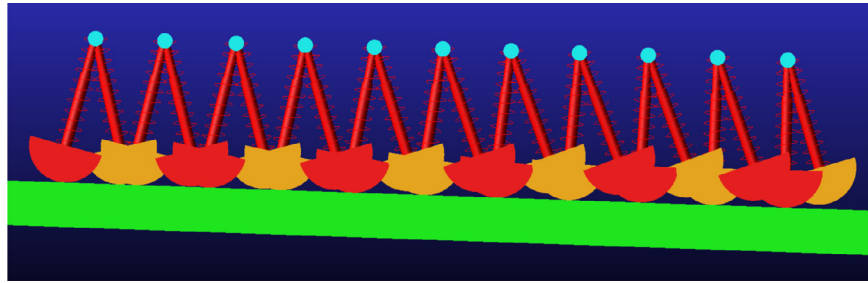


**Fig. 7.** Walking simulation of the simplified biped model in MSC Adams. Several snapshots show how the biped walks down the slope.

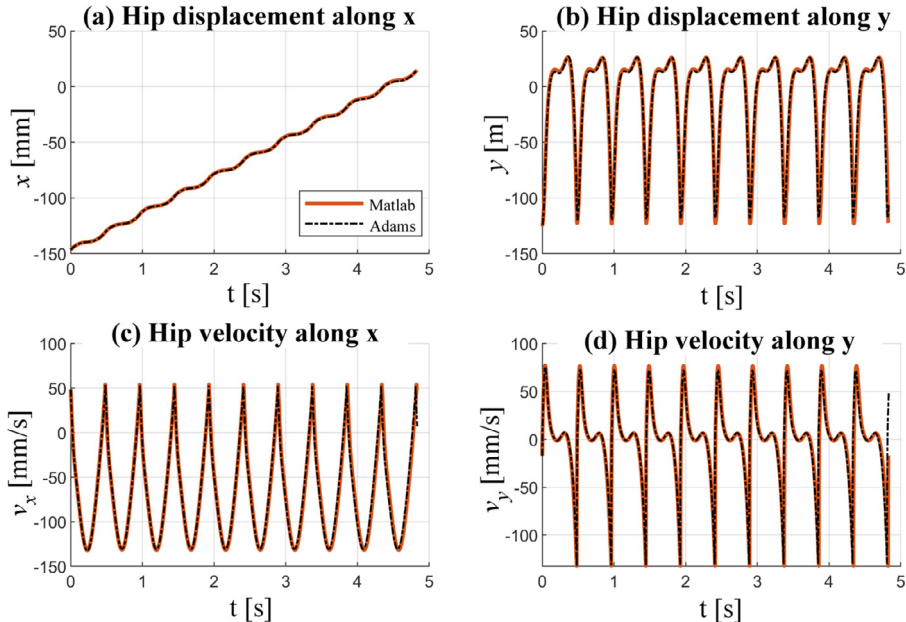


**Fig. 8.** Comparison between MATLAB and Adams results. The responses are almost identical. Hip displacement along the  $x$  and  $y$  directions (subplots (a) and (b) respectively) present a maximum difference of 0.3 mm. Hip velocity along the  $x$  and  $y$  directions (subplots (c) and (d)) present a maximum difference of 5 mm/s. After elimination of other possible causes, the small errors are attributed to integration tolerances.

#### 4. Discussion

Although it has been claimed in other studies that it is not possible to completely repeat the MATLAB simulation results in MSC Adams, see for example [23], here it is shown that the differences in the gait of the two models are negligible. Therefore, taking into consideration this closeness, the modelling decisions made so far are validated. Specifically, Lagrangian constraints are found to be an efficient mathematical tool for modelling contact between two bodies. Additionally, the parameter sets used in MSC ADAMS and presented here are recommended for simulations of similar systems.

This ascertainment will be employed next in the experimental prototype's development: the creation of a more detailed CAD model of the biped, based on the models studied so far. The CAD model can be verified for its dynamic resemblance to the previous models using MSC Adams, a necessary step before building and testing the real prototype.

#### 5. Biped robot design and validation

In this section, the detailed mechanical design of the NTUA biped is discussed. Specifically, a passive walker is designed in SolidWorks based on the simple models that have been studied in the previous sections. An interconnection between SolidWorks and MSC Adams is established, to verify via dynamics simulations the ability of the biped under development in achieving stable walking.

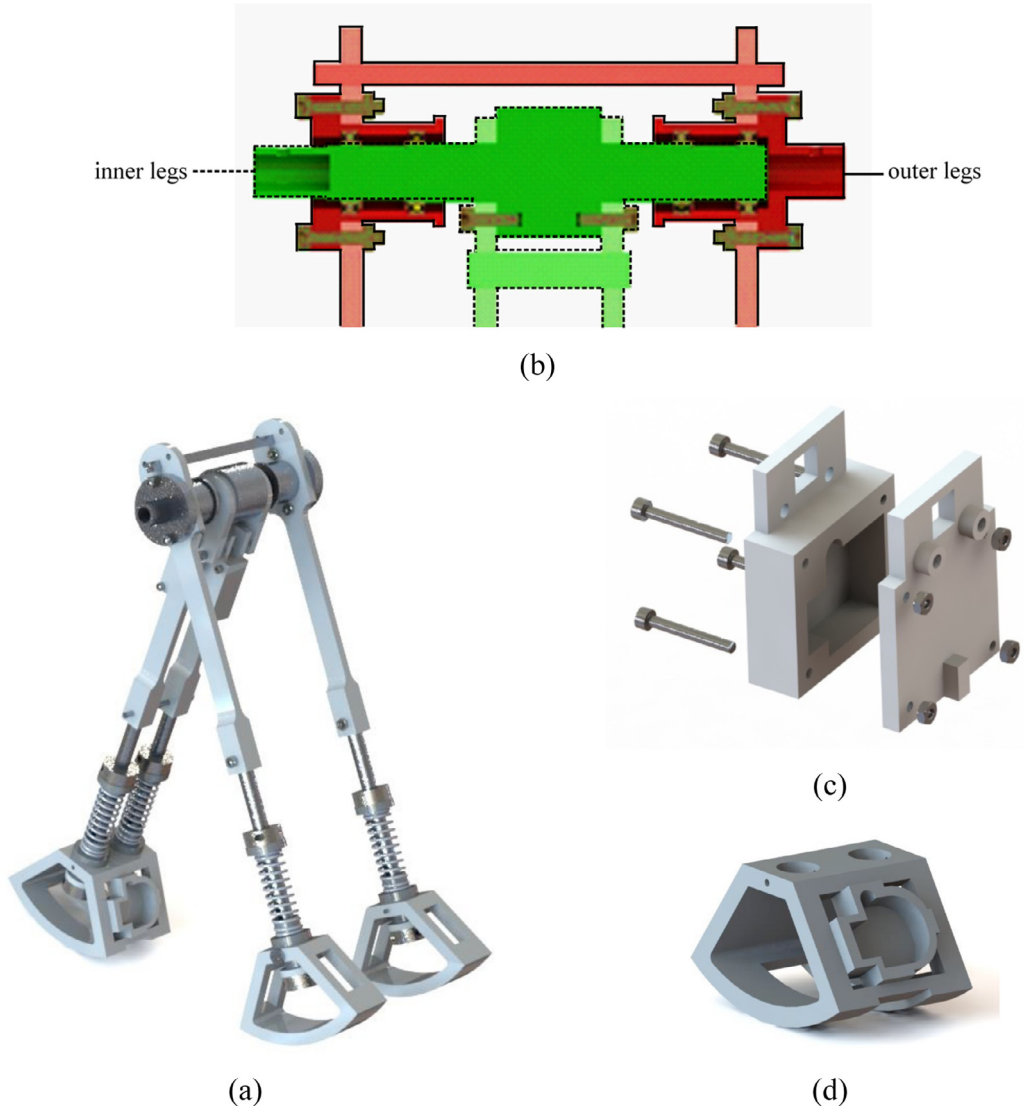


**Fig. 9.** (a) The detailed CAD design of the biped. (b) Frontal section view of the hip and rotational axes layout for the inner and outer legs. The inner legs that rotate along with the main shaft are marked in green. The outer legs, marked in red, are able to move independently with respect to the inner legs due to ball bearings. Other mechanical parts, such as bolts and bars that connect components can be distinguished in the section view of the hip. (c,d) Sensor sockets for the (c) hip-sensor and (d) the foot-sensor. (For interpretation of the references to colour in this figure legend, the reader is referred to the web version of this article.)

### 5.1. Mechanical design

The final robot design is presented in Fig. 9a. To enhance its resemblance to the planar models studied so far, the bipedal robot is designed to have paired inner and outer legs, allowing it to achieve planar motion without any supporting mechanism. One of the main goals of the design is to maintain the biped's structure, and its ability to perform stable passive walking.

For the biped's body, ABS plastic and aluminium were used primarily. These materials are readily available and easily configurable, and therefore the bipedal robot is built using the Lab's 3D printing and manufacturing facilities. Additionally, the use of ABS as a structural material facilitates the design of a lightweight robot, one that matches the mass distributions of the initial models. Moreover, the use of aluminium increases the strength of critically loaded parts. Leg compliance is achieved with the use of a mechanical spring in the lower part of the leg. The frictionless prismatic joint between leg and foot is achieved with the use of acetal, a low-friction, and low-wear material, as a sliding interface material. The damping elements of the model correspond to the material damping properties of the prototype.

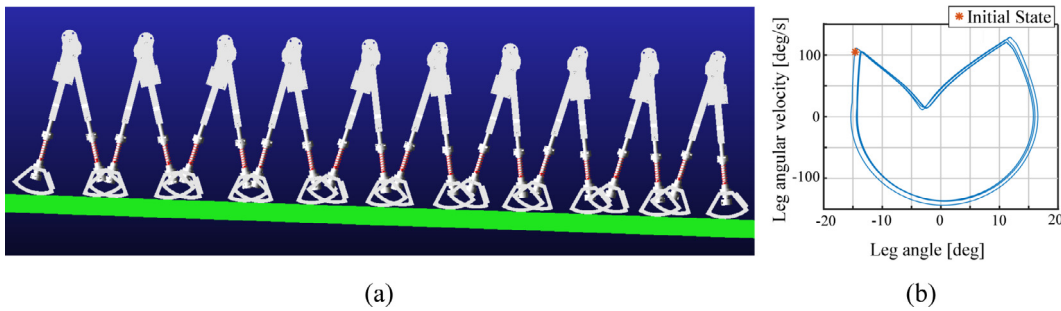


**Fig. 10.** (a) Digital twin biped model walking simulation, (b) leg angle phase space.

A main aspect of the design is the modularity of the construction. To this end, the hip and each of the legs consist of a number of components, which enables easy replacement in case of mechanical failure or changes in future designs. The independent rotation of the inner and outer legs around the hip axis is achieved with the use of ball bearings. The inner legs are rigidly attached to the main hip shaft, while the outer legs are attached on hollow tubes surrounding the shaft. The synchronization of each pair of legs is accomplished with the use of metallic rectangular beams on each side of the hip shaft. A section view of the hip shaft is presented in Fig. 9b. In the section view of the hip, all parts that rotate with the main shaft and the inner legs are marked in green and enclosed in a dashed outline, while parts that rotate along with the hollow tubes and the outer legs are marked in red and enclosed in a solid outline. Special sockets, shown in Fig. 9c and 9d, have been added in the hip and inner foot, to nest the IMU sensors that will be used for the experimental validation of the prototype. These locations will also be used as sampling points during the simulation of the CAD model in MSC Adams, to enable accurate comparison between model and prototype.

## 5.2. Digital twin design validation with MSC adams

The detailed 3D CAD model developed in SolidWorks was imported in MSC Adams and serves as a digital twin to the biped robot prototype. Dynamics simulations are conducted using the digital twin, as the last checkpoint prior to the manufacturing process. The digital biped is expected to walk similarly to the simpler models and to maintain its ability to perform passive gait; however, a few differences in the gait dynamics are expected due to the more complex geometric elements present in the final design. Simulation results are presented in this section.

Fig. 10a shows a few snapshots of the stable passive gait performed by the digital twin model. The biped is able to passively walk down the inclined plane in a stable gait. The gait stability can be observed in Fig. 10b, where the leg-angle phase space of the system is presented. The model is initially given the fixed-point initial conditions of the stable passive gait performed by the simpler models in MATLAB and Adams.

However, as can be observed, these initial conditions are not part of the digital twin's fixed-point trajectory: due to this, a transient phase during the first few steps appears, which eventually converges to its stable walking pattern. This slight difference in the shape of the stable trajectory of the digital twin and that of the simpler models is expected, considering the minor differences in the design, such as the inertial distribution of the different parts and materials used, and in the modelling, such as the replacement of the planar constraints by the double sets of legs.

## 6. Discussion

The results of the digital twin's simulation validate the previously developed models, as the biped maintains its basic design and its ability to perform fully passive and stable gait, in a trajectory very similar to the one observed in the initial stages of the study. This encourages the development of the experimental prototype to perform real-life experiments.

## 7. Experiment

The primary aims of the experimental procedure are to reproduce passive walking using a real prototype, to compare the results between experiment and simulations, and to determine the degree in which the proposed software and modelling decisions can be used to accurately model this type of system.

The bipedal prototype is built as a "twin" to its detailed digital design presented in Section 4 with minimal changes; the end result is presented in Fig. 11. In the prototype, a rubber cover is used on the feet to ensure that the static friction coefficient of the foot-ground contact is approximately 1, to match the modelling in MSC Adams. Moreover, the figure shows the position of the custom low-friction prismatic joint on the final prototype.

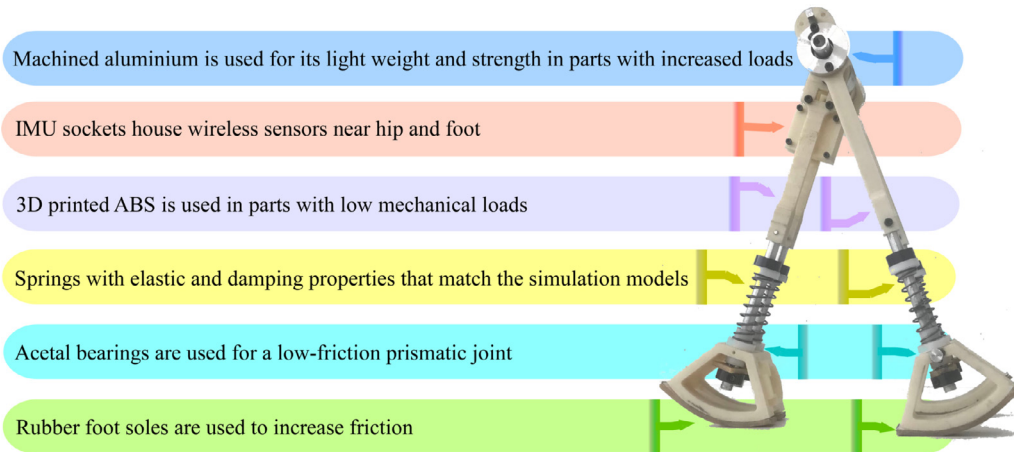


**Fig. 11.** The constructed biped robot prototype.

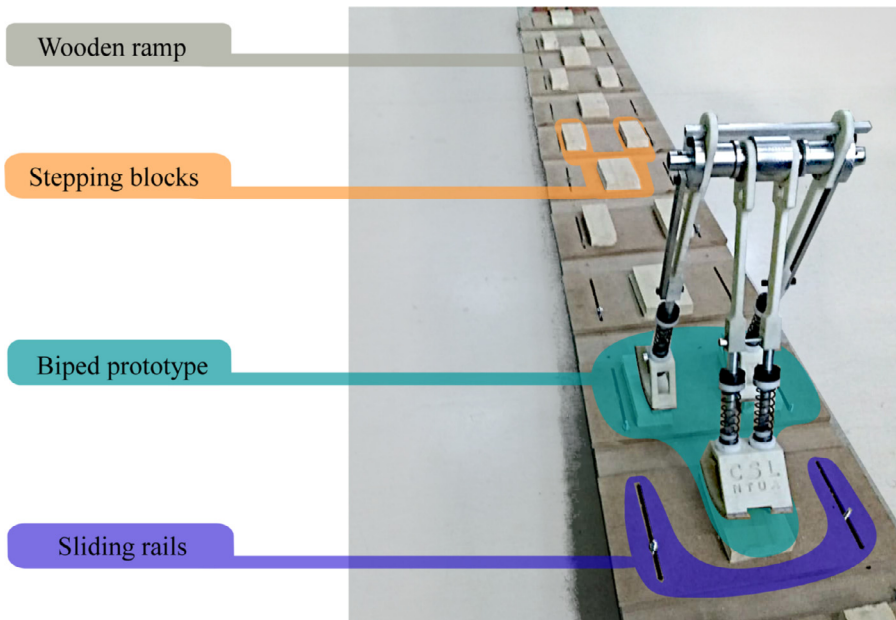


**Fig. 12.** Photo of biped prototype on the ramp.

### 7.1. Experimental Setup

**Fig. 12** shows the experimental setup, which consists of the constructed robot, a wooden ramp equipped with modular stepping blocks to avoid ground scuffing, and the IMU sensors attached in the previously specified positions for data acquisition. The ramp has a length of 2 meters, and a total of 11 stepping block sets. The slope of the ramp's inclination can be changed by adjusting its metal substrate, and the stepping blocks can be shifted forward and backward along their sliding rails, to accommodate a wide range of walking patterns.

The experimental setup is simple and easy to build. A downside of the setup is that the stepping blocks' position cannot be altered during an experiment, and therefore the step length of the gait must be previously known. This is not limiting for the present study, as there is enough simulation data to allow an educated guess of this type of gait determinant.

The experimental biped was found to be successful in replicating the passive gait found in the simulations previously performed. An important step of each experiment is ensuring that the initial conditions given to the biped are close enough to the stable trajectory that the biped converges towards it after a short transition phase. These should ideally match the values found by the use of simulations. The initial position of the biped can be configured with the adjustment of the ramp's stepping blocks. The desired initial velocities are more difficult to obtain without specifically designed equipment; however, this was considered unnecessary to develop as the biped easily converged to its stable gait after a well-rehearsed push.

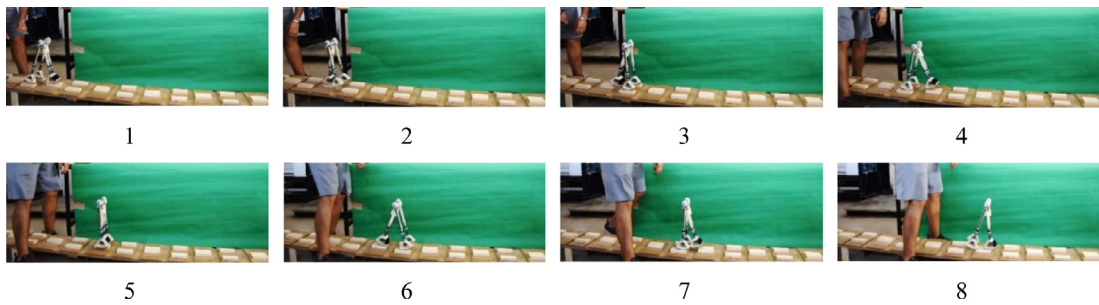


**Fig. 13.** Walking experiment of the experimental prototype.

The observed converging behaviour is attributed to the optimally stable dynamics of the biped's design and its robust basin of attraction to a stable gait trajectory, see [Table 1](#). This behaviour constitutes a validation of the design optimization for maximum stability, that was performed at the initial stages of the biped's development in MATLAB. In [Fig. 13](#), a series of snapshots are provided to visualize six consecutive steps of a passive walk.

Having ensured the biped's ability to perform a passive gait, the IMU sensors are employed to retrieve experimental data that will enable us to determine the convergence of the prototype's gait characteristics to the ones obtained through simulation. The complete experimental data acquisition and data retrieval process is discussed in detail next.

## 7.2. Experimental data acquisition

With a goal of comparing the numerical and multibody dynamics simulations performed in MATLAB and MSC Adams to their twin experimental prototype, one must choose to compare values that are easily sampled in both simulation and experiment, and that are representative of the system's dynamics. Such data are the biped's hip inertial accelerations and angular velocities, as they can be calculated easily in all digital models and can be acquired from the experimental prototype with the use of IMUs.

As previously discussed, the biped robot's passive dynamics are easily altered when the system's parameters change. Therefore, a data acquisition system must be developed that will not be intrusive with respect to the walking dynamics: it should be wireless to avoid the constraints imposed by data cables, and lightweight to ensure that the inertial characteristics of the biped remain intact. The data acquisition device selected for the experimental setup is the DA14583 IoT, manufactured by Dialog Semiconductors. The device features a 3-axial accelerometer, gyroscope, and magnetometer, integrated on a single 15 x 16 mm board along with various other environmental sensors. The device is also equipped with an ARM Cortex-M0 CPU, which allows the real-time processing of the sampled data, and a BLE module that enables wireless data transmission.

These sensors are the key elements of a custom-made, wireless, real-time data acquisition system that has been developed in our lab. The system consists of two parts: of a mobile one composed of a smartphone and IMU devices, and a static one composed of a computer which hosts a database for storing and retrieving the experimental data. The realization of a fully mobile subsystem allows a truly wireless setup as the user is not restricted to a confined space.

[Fig. 14](#) presents a schematic of the data acquisition system's topology. A smartphone application has been developed to employ the smartphone's BLE module and establish communication with the active IMUs. As the IMUs sample data, the smartphone uses its internet connection to post them in real-time to an SQL database, hosted on the static computer. To monitor the biped's gait dynamics, two IMUs have been mounted on the robot, inside custom-fitted sockets: one on the biped's foot and one close to the hip joint (also see [Fig. 9](#)).

[Fig. 15a](#) shows the IMU devices' body-fixed coordinate systems, as those are superposed on the biped's schematic, see [Fig. 15b,c](#). To facilitate the comparison process, special care has been taken to ensure that the simulation results obtained through MATLAB and MSC Adams have been sampled from points having the exact same position and orientation as the experimental prototype's sensors.

To ensure that the dynamics of the biped's gait are captured by the IMU devices, the latter are set to measure accelerations up to 4 g and angular velocities up to 2000 deg/s, both at a sampling rate of 100 Hz. This sampling rate is almost 50 times larger than the simulated walking frequency of 2.08 Hz.

## 7.3. Data retrieval

After each experiment, the data recorded can be retrieved from the SQL database. The dataset that corresponds to each experiment can be easily identified by the global timestamp accompanying each measurement. The retrieved data is then post-processed to eliminate some artefacts often introduced by data acquisition systems: one such example is the time-warping of some timestamps due to batch transfer protocols; another is data synchronization due to slight differences in sample sizes. The post-processed datasets can be loaded in MATLAB to enable direct comparison to the simulation results.

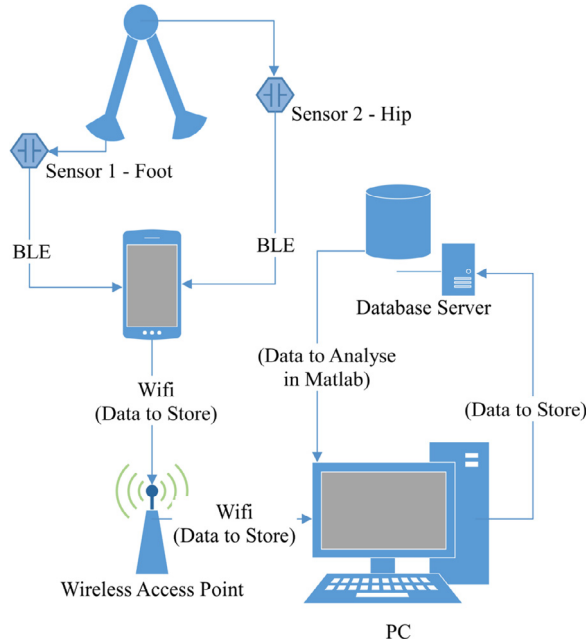


**Fig. 14.** Data acquisition system topology. The two IMUs, placed at the biped foot and hip, send sampled data to a smartphone application via BLE. The smartphone sends the data to the PC via WiFi over a local network. The host computer posts the sampled data in real-time to an SQL database, from which they can be retrieved for further analysis.

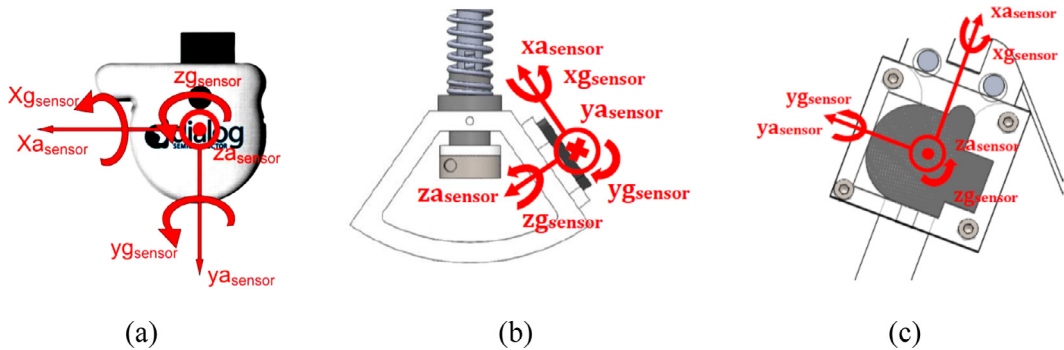


**Fig. 15.** IMU employed. (a) Sensor-based coordinate system, (b) transformed coordinate system of foot sensor, (c) transformed coordinate system of hip sensor.

#### 7.4. Results and comparison between experiment and simulation

A sufficient and representative dataset of the experimental results is obtained by conducting a series of 30 experiments with the prototype robot. In this way, the uncertainty revolving around the robot's response is reduced.

The results are compared to the simulation results of both the simplified and the detailed model. The aim is to compare directly the measurements coming from the data acquisition system: these are the accelerations and angular velocities measured by the IMUs. Different measurements could also be of interest: for example, the hip position in the x and y direction of motion proved to be an interesting point of comparison between the MATLAB and MSC Adams models. However, IMUs generally are known to introduce a measurement drift over time, and therefore the double integrations that would be needed in the hip trajectory calculation would introduce a considerable amount of accumulated error. To avoid this, the IMUs' acceleration and velocity measurements in their respective body-fixed coordinate systems are selected as the data to be compared between simulations and experiment.

This comparison is presented in Fig. 16, where the experimental data is compared to the simple and detailed Adams models. The results of the MATLAB simulation have been found to be effectively identical to the ones of the simple Adams model and as such have not been repeated in this comparison. The comparison in Fig. 16 showcases the major similarities and differences between the developed models and the robot prototype. The general repeatability of the data and the biped's ability to perform passive gait are indicated in the two plots: both the accelerations and velocity plots present a high degree

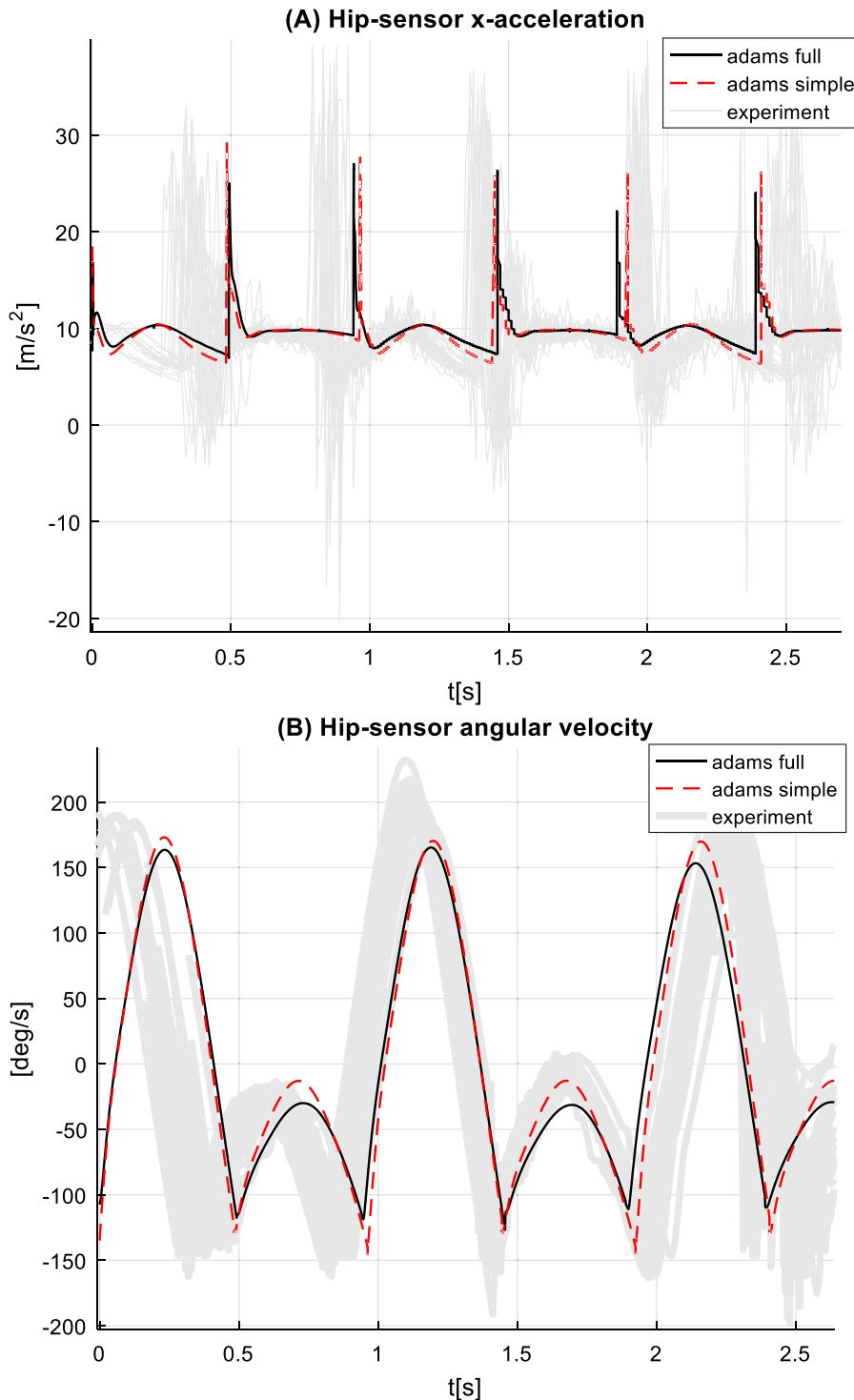


**Fig. 16.** Comparisons between real biped (experiment), its digital twin (Adams full), and simplified model (Adams simple). (a) the hip acceleration, (b) angular velocity. The simulation results of the simplified model (red dashed line) are almost identical with the simulation results of the detailed model (black line); the experiments indicate slight divergence (grey lines). (For interpretation of the references to colour in this figure legend, the reader is referred to the web version of this article.)

of resemblance in the general data trends between simulations and reality. Additionally, the data in both the acceleration and the angular velocity plots of both models and experiment are of the same order of magnitude and of considerable numerical convergence, indicating that there is high accuracy of the developed dynamics models. This is especially true for the acceleration plots, where a larger spike in the IMU's response to the heel strike impact was expected to be observed in the experimental data. Instead, both datasets present significant success in the model estimation of the robot dynamics.

On the other hand, it is observed that there is a slight difference in the step frequency between simulations and experiment: specifically, the lab prototype appears to walk slightly slower than the simulated models. This small difference can be attributed to the extra length added to the biped's legs due to the rubber outsoles, as a larger length generally leads to slower swing frequencies in pendulum-like systems. Another reason for this divergence could be the partial randomness in the initial velocity of the biped after each push at the beginning of each experiment. However, the difference in frequencies is not considered significant to question the validity of the models and their ability to simulate the passive gait of the biped prototype.

The data convergence also provides a positive insight about the approximation of the prototype's quality of manufacture, as it implies that the dynamic elements and geometry of the prototype truly correspond to the parameter values selected and used in the simulation models.

Finally, the whole set of the experimental data envelops the simulated ones, indicating that the developed models are validated for their ability to estimate the dynamic response of the biped robot, and to provide an accurate and reliable representation of the magnitude of the accelerations and velocities of the robot's gait, as well as an estimation of step frequency.

## 8. Conclusion

In this paper, the entire development and validation process for various models of a passive biped has been analysed. The process starts with the derivation of a simple mathematical model that describes the dynamic system and concludes with experimental trials using a built biped prototype. A detailed design loop between the two is also presented and discussed. To increase confidence in each step of this loop, gradual comparisons of the intermediate results have been held. Initially, the developed mathematical model was simulated, and its dynamics were studied. The second step was the mathematical model's translation to a simple 2D multibody dynamics model in a physics simulation environment, which provided a completely independent way to obtain the same results. Following this validation of both models by full convergence of their dynamics, a detailed design process took place to create a digital twin of the biped robot: a functional and detailed 3D CAD model. The digital twin was also simulated in a multibody simulation environment and its dynamic resemblance to the simpler models was verified. To close the loop, a biped prototype robot was manufactured as a twin of the 3D CAD model. This enabled us to conduct carefully designed experiments and to obtain data directly comparable across reality and multiple models in various simulation platforms. The high degree of resemblance across all data sources testifies to the validity of the developed models and the suitability of the various platforms in simulating the nonlinear, hybrid dynamics of passive biped walkers. Therefore, we recommend highly the developed framework for the design of similar experiments and propose that a carefully designed digital twin of a passive biped can be used with confidence in drawing safe conclusions about the real robot's dynamic response.

## Declaration of Competing Interest

The authors declare that they have no known competing financial interests or personal relationships that could have appeared to influence the work reported in this paper.

## References

- [1] T. McGeer, Passive dynamic walking, *Int. J. Rob. Res.* 9 (1990) 62–82, doi:[10.1177/027836499000900206](https://doi.org/10.1177/027836499000900206).
- [2] R.M. Alexander, A model of bipedal locomotion on compliant legs, *Philos. Trans. R. Soc. London. Ser. B Biol. Sci.* 338 (1992) 189–198, doi:[10.1098/rstb.1992.0138](https://doi.org/10.1098/rstb.1992.0138).
- [3] M. Garcia, A. Chatterjee, A. Ruina, M. Coleman, The simplest walking model: stability, complexity, and scaling, *J. Biomech. Eng.* 120 (1998) 281–288, doi:[10.1115/1.2798313](https://doi.org/10.1115/1.2798313).
- [4] B. Espiau, A. Goswami, Compass gait revisited, *IFAC Proc. Vol.* 27 (1994) 839–846, doi:[10.1016/s1474-6670\(17\)47405-2](https://doi.org/10.1016/s1474-6670(17)47405-2).
- [5] M. Alba, J.C.G. Prada, J. Meneses, H. Rubio, Center of percussion and gait design of biped robots, *Mech. Mach. Theory* 45 (2010) 1681–1693, doi:[10.1016/j.mechmachtheory.2010.06.008](https://doi.org/10.1016/j.mechmachtheory.2010.06.008).
- [6] C. Chevallereau, P. Wenger, Y. Aoustin, F. Mercier, N. Delanoue, P. Lucidarme, Leg design for biped locomotion with mono-articular and bi-articular linear actuation, *Mech. Mach. Theory* 156 (2021) 104138, doi:[10.1016/j.mechmachtheory.2020.104138](https://doi.org/10.1016/j.mechmachtheory.2020.104138).
- [7] A. Smyrli, M. Ghiassi, A. Kecskemethy, E. Papadopoulos, On the effect of semielliptical foot shape on the energetic efficiency of passive bipedal gait, in: *Proc. 2020 IEEE Int. Conf. Intell. Robot. Syst.*, 2020, pp. 6302–6307, doi:[10.1109/iros40897.2019.8967565](https://doi.org/10.1109/iros40897.2019.8967565).
- [8] S.H. Collins, A. Ruina, A bipedal walking robot with efficient and human-like gait, in: *Proc. 2005 IEEE Int. Conf. Robot. Autom.*, 2005, pp. 1983–1988, doi:[10.1109/ROBOT.2005.1570404](https://doi.org/10.1109/ROBOT.2005.1570404).
- [9] M. Wisse, A.L. Schwab, R.Q. van der Linde, F.C.T. van der Helm, How to keep from falling forward: elementary swing leg action for passive dynamic walkers, *IEEE Trans. Robot.* 21 (2005) 393–401, doi:[10.1109/TRO.2004.838030](https://doi.org/10.1109/TRO.2004.838030).
- [10] E. Corral, J. Meneses, C. Castejón, J.C. García-Prada, Forward and Inverse dynamics of the biped PASIBOT, *Int. J. Adv. Robot. Syst.* 11 (2014) 109, doi:[10.5772/58537](https://doi.org/10.5772/58537).
- [11] J. Meneses, C. Castejón, E. Corral, H. Rubio, J.C. García-Prada, Kinematics and dynamics of the quasi-passive biped “PASIBOT, *Stroj. Vestnik/Journal Mech. Eng.* 57 (2011) 879–887, doi:[10.5545/sv-jme.2010.210](https://doi.org/10.5545/sv-jme.2010.210).

- [12] V. Sangwan, A. Taneja, S. Mukherjee, Mech.Mach. Theory, Design of a robust self-excited biped walking mechanism, Elsevier Ltd (2004) 1385–1397, doi:[10.1016/j.mechmachtheory.2004.05.023](https://doi.org/10.1016/j.mechmachtheory.2004.05.023).
- [13] Z. Li, Z. Wu, Y. Zhao, Semi-active stable landing control for biped robot by using switching control, in: 2014 IEEE Int. Conf. Inf. Autom., 2014, pp. 740–745, doi:[10.1109/ICInFA.2014.6932750](https://doi.org/10.1109/ICInFA.2014.6932750).
- [14] C. Hubicki, A. Abate, P. Clary, S. Rezazadeh, M. Jones, A. Peekema, J. Van Why, R. Domres, A. Wu, W. Martin, H. Geyer, J. Hurst, Walking and running with passive compliance: lessons from engineering: a live demonstration of the ATRIAS biped, IEEE Robot. Autom. Mag. 25 (2018) 23–39, doi:[10.1109/MRA.2017.2783922](https://doi.org/10.1109/MRA.2017.2783922).
- [15] G. Carbone, H.O. Lim, A. Takanishi, M. Ceccarelli, Stiffness analysis of biped humanoid robot WABIAN-RIV, Mech. Mach. Theory 41 (2006) 17–40, doi:[10.1016/j.mechmachtheory.2005.05.001](https://doi.org/10.1016/j.mechmachtheory.2005.05.001).
- [16] M.S. Garcia, Stability, scaling, and chaos in passive-dynamic gait models, Cornell University Ithaca, NY, 1999.
- [17] S. Iqbal, X. Zang, Y. Zhu, J. Zhao, Bifurcations and chaos in passive dynamic walking: a review, Rob. Auton. Syst. 62 (2014) 889–909, doi:[10.1016/j.robot.2014.01.006](https://doi.org/10.1016/j.robot.2014.01.006).
- [18] S. Dallas, K. Machairas, E. Papadopoulos, A comparison of ordinary differential equation solvers for dynamical systems with impacts, J. Comput. Nonlinear Dyn. 12 (2017), doi:[10.1115/1.4037074](https://doi.org/10.1115/1.4037074).
- [19] N. Liu, J. Li, T. Wang, Passive walker that can walk down steps: simulations and experiments, Acta Mech. Sin. 24 (2008) 569–573, doi:[10.1007/s10409-008-0175-9](https://doi.org/10.1007/s10409-008-0175-9).
- [20] D. Koop, C.Q. Wu, Passive dynamic biped walking—part i: development and validation of an advanced model, J. Comput. Nonlinear Dyn. 8 (2013), doi:[10.1115/1.4023934](https://doi.org/10.1115/1.4023934).
- [21] M. Wisse, D.G.E. Hobbelin, A.L. Schwab, Adding an upper body to passive dynamic walking robots by means of a bisecting hip mechanism, IEEE Trans. Robot. 23 (2007) 112–123, doi:[10.1109/TRO.2006.886843](https://doi.org/10.1109/TRO.2006.886843).
- [22] H. Cao, Y. Wang, J. Zhu, Z. Ling, Dynamic simulation of passive walker based on virtual gravity theory, in: Lect. Notes Comput. Sci., Berlin, Heidelberg, Springer, 2009, pp. 1237–1245, doi:[10.1007/978-3-642-10817-4\\_124](https://doi.org/10.1007/978-3-642-10817-4_124).
- [23] T. Ylikorpi, J.-L. Peralta, A. Halme, Comparing passive walker simulators in Matlab and Adams, J. Struct. Mech. 44 (2011) 65–92.
- [24] M. Wisse, G. Feliksdal, J.V. Frankenhuizen, B. Moyer, Passive-based walking robot, IEEE Robot. Autom. Mag. 14 (2007) 52–62, doi:[10.1109/MRA.2007.380639](https://doi.org/10.1109/MRA.2007.380639).
- [25] S.M.H. Sadati, M. Borgheinejad, H. Fooladi, M. Naraghi, A.R. Ohadi, Optimum design, manufacturing and experiment of a passive walking biped: effects of structural parameters on efficiency, stability and robustness on uneven trains, Appl. Mech. Mater. 307 (2013) 107–111, doi:[10.4028/www.scientific.net/AMM.307.107](https://doi.org/10.4028/www.scientific.net/AMM.307.107).
- [26] X. Zang, J. Bai, Y. Zhu, J. Zhao, The global stability analysis of passive biped robot based on gradual point mapping – cell mapping method, in: 2013 2nd Int. Symp. Instrum. Meas. Sens. Netw. Autom., 2013, pp. 800–804, doi:[10.1109/IMNSA.2013.6743398](https://doi.org/10.1109/IMNSA.2013.6743398).
- [27] J. Zhao, X. Liu, X. Zang, X. Wu, A PD control scheme for passive dynamic walking based on series elastic actuator, in: 2012 IEEE Int. Conf. Mechatronics Autom., 2012, pp. 255–260, doi:[10.1109/ICMA.2012.6282851](https://doi.org/10.1109/ICMA.2012.6282851).
- [28] E. Corral, M.J.G. García, C. Castejon, J. Meneses, R. Gismeros, Dynamic Modeling of the Dissipative Contact and Friction Forces of a Passive Biped-Walking Robot, Appl. Sci. 10 (2020) 2342, doi:[10.3390/app10072342](https://doi.org/10.3390/app10072342).
- [29] F.Marques Corral, M.J. Gómez García, P. Flores, J.C. García-Prada, Passive walking biped model with dissipative contact and friction forces, in: Mech. Mach. Sci., Netherlands, Springer, 2019, pp. 35–42, doi:[10.1007/978-3-319-98020-1\\_5](https://doi.org/10.1007/978-3-319-98020-1_5).
- [30] A. Smyrli, G.A. Bertos, E. Papadopoulos, Efficient stabilization of zero-slope walking for bipedal robots following their passive fixed-point trajectories, in: Proc. - IEEE Int. Conf. Robot. Autom., 2018, pp. 5733–5738, doi:[10.1109/ICRA.2018.8460845](https://doi.org/10.1109/ICRA.2018.8460845).
- [31] K.H. Hunt, F.R.E. Crossley, Coefficient of restitution interpreted as damping in vibroimpact, J. Appl. Mech. Trans. ASME. 42 (1975) 440–445, doi:[10.1115/1.3423596](https://doi.org/10.1115/1.3423596).
- [32] P. Flores, M. Machado, M.T. Silva, J.M. Martins, On the continuous contact force models for soft materials in multibody dynamics, Multibody Syst. Dyn. 25 (2011) 357–375, doi:[10.1007/s11044-010-9237-4](https://doi.org/10.1007/s11044-010-9237-4).
- [33] H. Safaeifar, A. Farshidianfar, A new model of the contact force for the collision between two solid bodies, Multibody Syst. Dyn. 50 (2020) 233–257, doi:[10.1007/s11044-020-09732-2](https://doi.org/10.1007/s11044-020-09732-2).
- [34] G. Wang, C. Liu, Further investigation on improved viscoelastic contact force model extended based on hertz's law in multibody system, Mech. Mach. Theory 153 (2020) 103986, doi:[10.1016/j.mechmachtheory.2020.103986](https://doi.org/10.1016/j.mechmachtheory.2020.103986).
- [35] J. Zhang, W. Li, L. Zhao, G. He, A continuous contact force model for impact analysis in multibody dynamics, Mech. Mach. Theory. 153 (2020) 103946, doi:[10.1016/j.mechmachtheory.2020.103946](https://doi.org/10.1016/j.mechmachtheory.2020.103946).
- [36] V. Vasilopoulos, I. Paraskevas, E. Papadopoulos, Monopod hopping on compliant terrains, Robot. Autonom. Syst. 102 (Issue C) (2018) 13–26, doi:[10.1016/j.robot.2018.01.004](https://doi.org/10.1016/j.robot.2018.01.004).
- [37] F. Marques, P. Flores, J C Pimenta Claro, H.M. Lankarani, Modeling and analysis of friction including rolling effects in multibody dynamics: a review, Multibody Syst. Dyn. 45 (2019) 223–244, doi:[10.1007/s11044-018-09640-6](https://doi.org/10.1007/s11044-018-09640-6).
- [38] F. Marques, P. Flores, J C Pimenta Claro, H.M. Lankarani, A survey and comparison of several friction force models for dynamic analysis of multibody mechanical systems, Nonlinear Dyn. 86 (2016) 1407–1443, doi:[10.1007/s11071-016-2999-3](https://doi.org/10.1007/s11071-016-2999-3).
- [39] E. Pennestrì, V. Rossi, P. Salvini Pier, P. Valentini, Review and comparison of dry friction force models 83 (4) (2016) 1785–1801, doi:[10.1007/s11071-015-2485-3](https://doi.org/10.1007/s11071-015-2485-3).